Hindawi
Advances in Civil Engineering
Volume 2019, Article ID 7167802, 14 pages
https://doi.org/10.1155/2019/7167802

Research Article

Rotational Failure Mechanism for Face Stability of Circular Shield Tunnels in Frictional Soils

Yuan Zhou,[1] Yuming Zhu,[2] Shumao Wang,[3] Hu Wang,[2] and Zhengxing Wang[4]

[1]*Ph.D, Key Laboratory of Ministry of Education for Geomechanics and Embankment Engineering, Hohai University, Nanjing 210098, China*
[2]*Master Student, Key Laboratory of Ministry of Education for Geomechanics and Embankment Engineering, Hohai University, Nanjing 210098, China*
[3]*Ph.D, East China Electric Power Design Institute of China Power Engineering Consulting Group, Shanghai 200063, China*
[4]*Ph.D, Senior Engineer, Nantong City Construction Group Co., Ltd., Nantong 226000, China*

Correspondence should be addressed to Yuming Zhu; geoyumingzhu@gmail.com

Received 12 November 2018; Revised 26 January 2019; Accepted 12 February 2019; Published 7 March 2019

Academic Editor: Giovanni Garcea

Face stability analyses of shield-driven tunnels are often carried out to determine the required support pressure on the tunnel face. Although various three-dimensional mechanisms have been proposed for circular faces of tunnels in frictional and/or cohesive soils to obtain the limit support pressure, the most critical one has not yet been found. Based on a rotational failure mechanism for the frictional soils, this paper modifies the circular cross section as an ellipse to make the generating collapse surface inscribe the entire circular tunnel face. Using the kinematical approach of limit analysis yields an upper bound to the limit support pressure. Through comparisons with the existing results in the literature, the improved mechanism can better estimate the upper bound and is very similar to the observed failures in the experimental tests. The influences of the pore water pressure are also included in the stability analysis of tunnel faces. Calculated upper-bound solutions are presented in a condensed form of charts for convenient use in practice.

1. Introduction

Shield machines have been widely used for excavations of tunneling in loose grounds above or below the groundwater table. In the built-up areas, the tunnel face has to be adequately supported to prevent the excessive settlement at the ground. Different support methods are utilized in practice, such as compressed air, bentonite slurry, and earth pressure. Face stability analyses are often conducted to determine the required support pressure based on the limit equilibrium (LE), the limit analysis (LA), and the finite element (FE) or the finite difference (FD) methods. The face of most shield-driven tunnels is circular, and its stability should be analyzed in three-dimensional (3D) conditions. The numerical FE/FD method has advantage on the complex geometry of 3D problems, especially for modelling. The analytical LE/LA methods need to develop a 3D failure mechanism of the tunnel face in advance. The criticality of their calculated support pressure depends on the developed mechanism. Therefore, the construction of the 3D mechanism is of importance in the stability analysis of tunnel faces.

Horn [1] earlier proposed a wedge-prism model based on the silo theory and then solved LE equations to yield the limit support pressure. This model assumes the circular tunnel face as a square with slides corresponding to the tunnel diameter. It is further improved by Anagnostou and Kovári [2, 3] and Chen et al. [4] to involve the influences of pore water pressures (PWP) and soil arching effects. Compared with the LE solutions, the LA method based on the theorem of soil plasticity is more rigorous to yield the upper or lower bound of the limit load. Numerous 3D stability analyses of tunnel faces have been conducted in the

LA, especially for the upper-bound (UB) solutions. Unlike the lower-bound solutions, UB solutions are more critical for the determination of the support pressure on the tunnel face against the active collapse or passive blowout. To obtain the upper bound, a kinematically admissible velocity field needs to be proposed for the material with associated flow rule. For purely cohesive soils, Klar et al. [5] used the Tresca yield criterion to obtain the closed-form solution for the 3D deformation field. Mollon et al. [6] established continuous velocity fields, which can better estimate the upper bounds. However, it is difficult to present a velocity field for frictional soils obeying the Mohr–Coulomb yield criterion. Leca and Dormieux [7] proposed a 3D failure mechanism consisting of one or two conical blocks, and then Mollon et al. [8, 9] modified it using a multiblock model to obtain more critical support pressures. Many researchers [10–21] further developed the mechanism and investigated some effects, such as seepage forces, reinforcement, nonhomogeneous soils, and longitudinal gradient of tunnels. However, these mechanisms are limited to translational failures in frictional soils.

With the help of the advanced measurements and image processing techniques, such as X-ray and CT scanners [22], digital image correlation (DIC), or particle image velocimetry (PIV) [23–27], the 3D failure behavior of the tunnel face can be clearly recorded in the experimental tests. The observed results are useful for improvements of the failure mechanism. The measured results of Takano et al. [22] demonstrate the rotational movements for tunnel face failures in frictional soils. Subrin and Wong [28] considered the rotational movements of the tunnel face in cohesive frictional soils and proposed a rotational failure mechanism defined by two log spirals. The derived UB solutions of the support pressure have good agreements with the FE results of Wong and Subrin [29] and the experimental results measured by Berthoz et al. [30]. Similar to the translational failure mechanisms of Leca and Dormieux [7] and Mollon et al. [8], the area inscribed to the circular tunnel face has an elliptical shape in the rotational mechanism, which cannot cover the entire face. The striking results on the failure surface are not consistent with the observed results in the experimental tests of Takano et al. [22]. Recently, Mollon et al. [9] proposed a new rotational failure mechanism for circular faces of tunnels in frictional soils. A spatial discretization method is adopted to make the failure surface entirely passing through the circular tunnel face. The presented comparisons demonstrate that the presented mechanism can yield better upper bounds to the support pressure in the LA. The rotational mechanism has been further used for many other problems [31–35], such as nonhomogeneous soils, pore water pressures, reinforcement, noncircular tunnel faces, probabilistic evaluation, and rock tunnels. These developments indicate the efficiency of the presented discretization method on the 3D geometrical construction.

The purpose of this study is to improve the rotational failure mechanism of Subrin and Wong [28] for circular faces of tunnels in frictional and/or cohesive soils. The cross section of the 3D mechanism is modified as an ellipse, to avoid the inscribed elliptical area to the circular tunnel face. Using the kinematic LA method, the least UB solutions of the support pressure are obtained through an optimization procedure. The PWP effects are also included in the stability analyses. Comprehensive comparisons are made to verify the criticality of the improved 3D mechanism. Finally, these calculated UB solutions are presented in some stability charts for convenient use in practice.

2. Three-Dimensional Rotational Failure Mechanism

2.1. Definition of the Problem. Figure 1 illustrates the notations and conventions used in formulating the 3D stability analysis of tunnel faces. A circular shield-driven tunnel with a diameter of D is advancing in homogeneous soil stratums. The cover depth from the ground surface to the tunnel crown is denoted as C. The groundwater table is located at a height of H_w from the tunnel crown. The soil unit weight is γ. The simple Mohr–Coulomb failure criterion is adopted for the shear strength of soils, and the cohesion and internal friction angle can be denoted as c and φ, respectively. There is a support pressure (σ_{tc}) to prevent the tunnel face from active collapse. The support pressure is constant for compressed air. A rotational failure mechanism is proposed here to estimate the required support pressure against the tunnel face collapse. The face collapse only occurs below the ground surface. The case of the face blowout is not considered in this study.

2.2. Geometry of the Failure Surface. In the framework of limit analysis, an upper bound of the support pressure on tunnel faces can be obtained from the kinematic approach. A kinematically admissible velocity field describing the possible failure must satisfy both of the flow rule associated with the yield condition and the velocity boundary conditions. The failure of the circular tunnel face is axisymmetric in 3D conditions. Drescher [36] presented the characteristic relations of the axisymmetric velocity field, in which the velocity jump across a strong discontinuity is inclined at an angle φ. The velocity discontinuity satisfying the requirements is a straight line or a log spiral. The straight line is often used for translational failure mechanism in cohesionless soils, such as the classical wedge model generated by Horn [1] and the conical block model proposed by Leca and Dormieux [7]. The log spiral is more suitable for the rotational failure mechanism in frictional soils, as presented by Subrin and Wong [28] and Mollon et al. [37]. Therefore, the log-spiral line is also employed here to construct the rotational failure mechanism in 3D conditions.

The profile of the failure mechanism on the symmetry plane is bounded by two log-spiral lines, EF,

$$r(\theta) = r_0 e^{(\theta-\theta_0)\tan\varphi}, \tag{1}$$

and EF':

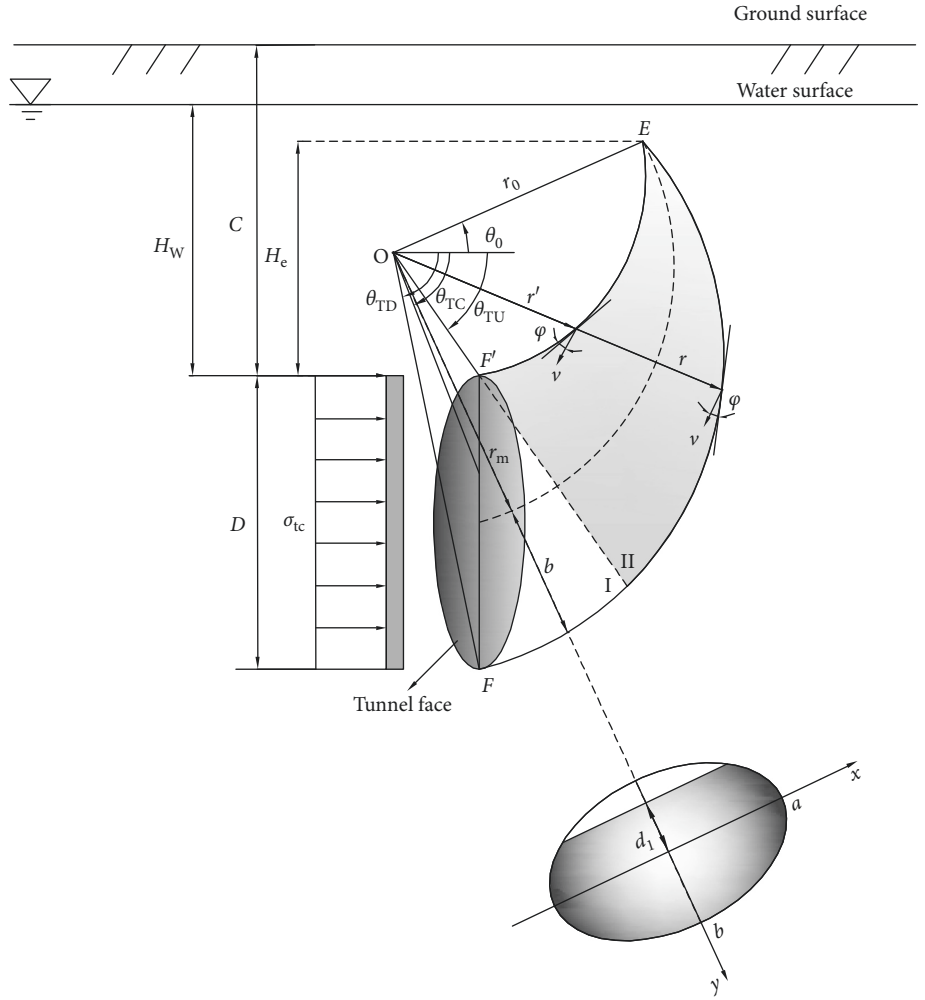

Figure 1: Central cross section of 3D rotational failure mechanism for circular tunnel face.

$$r'(\theta) = r_0 e^{-(\theta-\theta_0)\tan\varphi}, \tag{2}$$

where the radius r_0 and angle θ_0 are illustrated in Figure 1. The cross section of the failure mechanism is assumed as an ellipse, which can make the cross section on the vertical tunnel face consistent with the entire circular tunnel face. The ellipse can be expressed as

$$\frac{x^2}{a^2} + \frac{y^2}{b^2} = 1, \tag{3}$$

where a local coordinate system (x, y) is introduced for each cross section and shown in Figure 1. The x-axis is perpendicular to the plane of the symmetry plane. The parameters a and b are the semimajor and semiminor axes of the ellipse, respectively. The shape of the failure surface is generated by rotating an ellipse of increasing semiminor axis b about an axis passing through point O outside the ellipse. The centerline of the curvilinear cone from the rotating axis, r_m is

$$r_m = \frac{r + r'}{2}. \tag{4}$$

The increasing semiminor axis b can be expressed as

$$b = \frac{r - r'}{2}. \tag{5}$$

Using an eccentricity e, we can obtain the semimajor axis of the ellipse as

$$a = \frac{b}{\sqrt{1 - e^2}}. \tag{6}$$

In the zone I next to the tunnel face (Figure 1), the rotating angle θ ranges from θ_{TU} to θ_{TD}. The cross section of the failure mechanism on the tunnel face must be identical to the circle with tunnel diameter D. Based on the relationship, the eccentricity of the elliptical cross section can be obtained as

$$e = \sqrt{1 - \frac{4\left(b^2 - d_1^2\right)}{D^2 - 4d_2^2}}, \tag{7}$$

where parameters d_1 and d_2 are

$$d_1 = r_0 e^{(\theta_{TD}-\theta_0)\tan\varphi}\frac{\cos\theta_{TD}}{\cos\theta} - r_m,$$

$$d_2 = r_0 e^{(\theta_{TD}-\theta_0)\tan\varphi}\cos\theta_{TD}\left(\tan\theta - \frac{\tan\theta_{TU}+\tan\theta_{TD}}{2}\right). \tag{8}$$

Angles θ_{TU} and θ_{TD} are shown in Figure 1. From the geometrical and trigonometric relations, the radius r_0 and the angle θ_{TD} can be determined by the angles θ_0 and θ_{TU} as

$$r_0 e^{(\theta_{TD}-\theta_0)\tan\varphi}\sin\theta_{TD} - r_0 e^{-(\theta_{TU}-\theta_0)\tan\varphi}\sin\theta_{TU} - D = 0,$$
$$r_0 e^{(\theta_{TD}-\theta_0)\tan\varphi}\cos\theta_{TD} - r_0 e^{-(\theta_{TU}-\theta_0)\tan\varphi}\cos\theta_{TU} = 0. \tag{9}$$

The eccentricity of zone I is defined here, in order to make the interface of the tunnel face and the rotating plane conform to a whole circular face. For the remaining zone II of the failure mechanism ($\theta_0 \le \theta < \theta_{TU}$), the ellipse in the cross section is assumed to gradually degenerate as a circle at $\theta = \theta_0$, where the eccentricity $e = 0$. The eccentricity is varying with the angle θ as

$$e = e_0\left[1 - \left(\frac{\theta-\theta_{TU}}{\theta_0-\theta_{TU}}\right)^{\eta}\right], \tag{10}$$

where e_0 is the eccentricity of the elliptic cross section at $\theta = \theta_{TU}$, which makes the surface smooth. Parameter η is the coefficient of the power function. When $\eta = 1$, the eccentricity decreases linearly with angle θ.

3. Upper-Bound Solutions of Support Pressure on Tunnel Face

3.1. Formula. Using the kinematically admissible velocity field, we can obtain an upper bound on the limit support pressure of tunnel faces by equating the rate of work done by the external forces to the internal rate of dissipation. In the failure mechanism, the rigid body with the shape of curvilinear cone rotates about the axis passing through point O. The linear velocity v can be expressed as

$$v = (r_m + y)\omega, \tag{11}$$

where ω is the angular velocity and the infinitesimal volume element is

$$dV = dx\,dy\,(r_m + y)\,d\theta. \tag{12}$$

Then, the work rate of the soil weight can be written as

$$W_\gamma = \gamma\int_V v\cos\theta\,dV. \tag{13}$$

The overall failure mechanism is divided into two parts, as the denoted zone I and zone II in Figure 1. Using equation (13) into the two parts, we can calculate the corresponding work rate of the soil weight, $W_{\gamma 1}$ and $W_{\gamma 2}$, respectively. Their expressions are given as

$$\begin{aligned} W_{\gamma 1} = 2\omega\gamma\Bigg[&\int_{\theta_{TU}}^{\theta_{TC}}\int_0^a\int_{-\sqrt{b^2-(b^2/a^2)x^2}}^{\sqrt{b^2-(b^2/a^2)x^2}} (r_m+y)^2\cos\theta\,dy\,dx\,d\theta \\ &- \int_{\theta_{TU}}^{\theta_{TC}}\int_0^{\sqrt{a^2-(a^2/b^2)d_1^2}}\int_{-\sqrt{b^2-(b^2/a^2)x^2}}^{d_1} (r_m+y)^2 \\ &\cdot \cos\theta\,dy\,dx\,d\theta \\ &+ \int_{\theta_{TC}}^{\theta_{TD}}\int_0^{\sqrt{a^2-(a^2/b^2)d_1^2}}\int_{d_1}^{\sqrt{b^2-(b^2/a^2)x^2}} (r_m+y)^2 \\ &\cdot \cos\theta\,dy\,dx\,d\theta\Bigg] = 2\omega\gamma f_{\gamma 1}, \\ W_{\gamma 2} = 2\omega\gamma &\int_{\theta_0}^{\theta_{TU}}\int_0^a\int_{-\sqrt{b^2-(b^2/a^2)x^2}}^{\sqrt{b^2-(b^2/a^2)x^2}} (r_m+y)^2\cos\theta\,dy\,dx\,d\theta \\ = 2\omega\gamma &f_{\gamma^2}, \end{aligned} \tag{14}$$

where angle θ_{TC} can be obtained from the geometrical relation as

$$\begin{aligned} &r_0 e^{(\theta_{TD}-\theta_0)\tan\varphi}\cos\theta_{TD} \\ &= \frac{r_0 e^{(\theta_{TC}-\theta_0)\tan\varphi} + r_0 e^{-(\theta_{TC}-\theta_0)\tan\varphi}}{2}\cos\theta_{TC}. \end{aligned} \tag{15}$$

Following the same procedure, the rate of work done by the support pressure can also be calculated over the circular tunnel face and expressed as

$$\begin{aligned} W_{\sigma_{tc}} = -2\omega\sigma_{tc}&\int_{\theta_{TU}}^{\theta_{TD}}\int_0^{\sqrt{a^2-(a^2/b^2)d_1^2}}\left[r_0 e^{(\theta_{TD}-\theta_0)\tan\varphi}\frac{\cos\theta_{TD}}{\cos\theta}\right]^2 \\ &\cdot \tan\theta\,dx\,d\theta = -2\omega\sigma_{tc}f_{tc}. \end{aligned} \tag{16}$$

The rate of internal energy dissipated over the velocity discontinuity surface S can be calculated as

$$D_s = c\int_S v\cos\varphi\,dS, \tag{17}$$

where the infinitesimal surface element of the failure surface is expressed as

$$dS = \sqrt{1 + \frac{a^2y^2}{b^4 - b^2y^2}}\,dy\,(r_m + y)\frac{d\theta}{\cos\varphi}. \tag{18}$$

For the two parts of the failure surface, the rate of work dissipation D_{s1} and D_{s2} can be, respectively, written as

$$\begin{aligned} D_{s1} &= 2\omega c\int_{\theta_{TU}}^{\theta_{TD}}\int_{d_1}^{b}(r_m+y)^2\sqrt{1+\frac{a^2y^2}{b^4-b^2y^2}}\,dy\,d\theta = 2\omega c f_{s1}, \\ D_{s2} &= 2\omega c\int_{\theta_0}^{\theta_{TU}}\int_{-b}^{b}(r_m+y)^2\sqrt{1+\frac{a^2y^2}{b^4-b^2y^2}}\,dy\,d\theta = 2\omega c f_{s2}. \end{aligned} \tag{19}$$

Based on the energy balance, the limit support pressure can be determined and expressed in a dimensionless form:

$$\frac{\sigma_{tc}}{\gamma D} = N_\gamma - \frac{c}{\gamma D} N_c, \tag{20}$$

where the coefficients N_γ and N_c can be written as

$$N_\gamma = \frac{f_{\gamma 1} + f_{\gamma 2}}{D f_{tc}}, \qquad N_c = \frac{f_{s1} + f_{s2}}{f_{tc}}. \tag{21}$$

When the PWP influences are included to obtain the support pressure, the rate of work due to the seepage and buoyancy forces within the soil volume should be included in the energy balance. As presented by Michalowski [38] and Michalowski and Nadukuru [39], the rate of work done by PWP can be reduced because of the assumption on the rigid body of the soil mass as

$$W_u = -\int_S uv \sin\varphi \, dS, \tag{22}$$

where u is the magnitude of the PWP along the failure surface. During the excavation of the shield-driven tunnel, the distribution on PWP is complicated. To investigate the effects of the PWP on the support pressure, an approximate method is employed here to estimate the PWP using a coefficient r_u, which is defined by Bishop and Morgenstern [40] as

$$u = r_u \gamma h_w, \tag{23}$$

where h_w is the depth of the failure surface below the groundwater table. Using equation (22), we can calculate the rate of work done by PWP for part I and II, respectively:

$$W_{u1} = 2\omega r_u \gamma \int_{\theta_{TU}}^{\theta_{TD}} \int_{d_1}^{b} (r_m + y)^2 \sqrt{1 + \frac{a^2 y^2}{b^4 - b^2 y^2}} \tan\varphi \cdot \left[(r_m + y)\sin\theta - r_0 e^{-(\theta_{TU} - \theta_0)\tan\varphi} \sin\theta_{TU} + H_w\right] dy \, d\theta = 2\omega r_u \gamma f_{u1},$$

$$W_{u2} = 2\omega r_u \gamma \int_{\theta_0}^{\theta_{TU}} \int_{-b}^{b} (r_m + y)^2 \sqrt{1 + \frac{a^2 y^2}{b^4 - b^2 y^2}} \tan\varphi \cdot \left[(r_m + y)\sin\theta - r_0 e^{-(\theta_{TU} - \theta_0)\tan\varphi} \sin\theta_{TU} + H_w\right] dy \, d\theta = 2\omega r_u \gamma f_{u2}. \tag{24}$$

Including the rate of work done by PWP into the energy balance, we can obtain the support pressure as

$$\frac{\sigma_{tc}}{\gamma D} = N_\gamma + r_u N_u - \frac{c}{\gamma D} N_c, \tag{25}$$

where the coefficient N_u is

$$N_u = \frac{f_{u1} + f_{u2}}{D f_{tc}}. \tag{26}$$

3.2. Optimization Procedure. For a given problem (i.e., tunnel diameter D, cover depth C, soil density γ, soil cohesion c, internal friction angle φ, and the possible PWP coefficient r_u), using the balance equation, we can find the maximum value of the support pressure against the face collapse through an optimization procedure. The independent variables describing the 3D failure surface are angles θ_0 and θ_{TU}. In the search for the maximum value of σ_{tc}, the optimization procedure is carried out until the band widths of the angles reduce to 0.01°. In addition, the coefficient η defined in equation (10) is selected as $\eta = 10$ in the calculations. Through numerous tests, when the coefficient η is more than 5, the difference is negligent, as shown in Figure 2.

4. Results and Discussions

4.1. Comparisons with the Existing Results. Various mechanisms have been developed to determine the upper bounds of the support pressure. These UB solutions are also given here for validating the presented failure mechanism of this study. For the case of the cohesive frictional soils shown in Figure 3(a), the result derived from this study is more critical than other UB solutions. The required support pressure remains constant with the ratio of C/D. Because of the arching effects, the induced collapses are not reaching the ground surface, i.e., $H_e < C$. The same examples are also used by numerical FD methods [14, 41], and their results are given for comparisons, as shown in Table 1. The numerical results are smaller than those of this study. Based on the observed geometry of the numerically obtained failures, Zhang et al. [14] improved the existing multiblock mechanism of Mollon et al. [8] and then obtained more critical support pressure than that given by Mollon et al. [8]. However, the improved multiblock mechanism is still less critical than the presented rotational mechanism of this study.

For the purely frictional soil, it can be seen from Figure 3(b) that the calculated pressures are larger than other results for $\varphi = 20°$, but very closer to the results of Mollon et al. [37] for $\varphi = 40°$. It indicates that the presented mechanism can better estimate the UB solution. The wedge model proposed by Horn [1] is often used to estimate the required support pressure of tunnel face in the cohesionless soil. Chen et al. [4] considered the soil arching effects and then improved the classic mechanism. The limit support pressure is calculated by the LE method for different ratios of C/D, as shown in Figure 4(a). Because the present mechanism is not allowed to reach the ground surface, the obtained support pressure is independent on the cover depth. It can be seen that UB solutions of this study are close to the LE

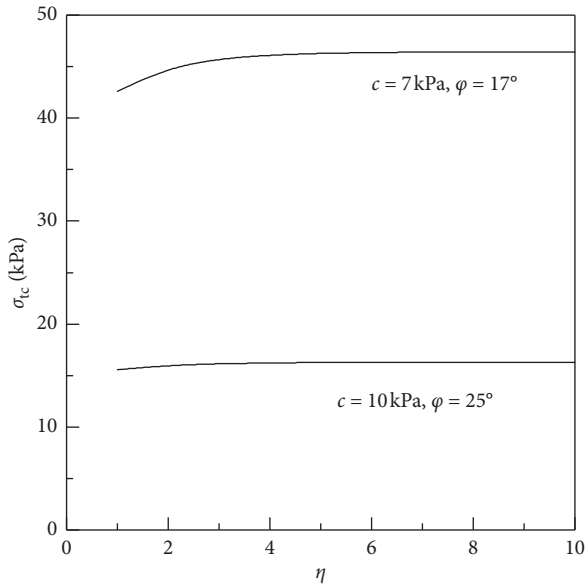

Figure 2: Influence of the coefficient η on the critical results ($D = 10$ m, $C = 10$ m, and $\gamma = 18$ kN/m^3).

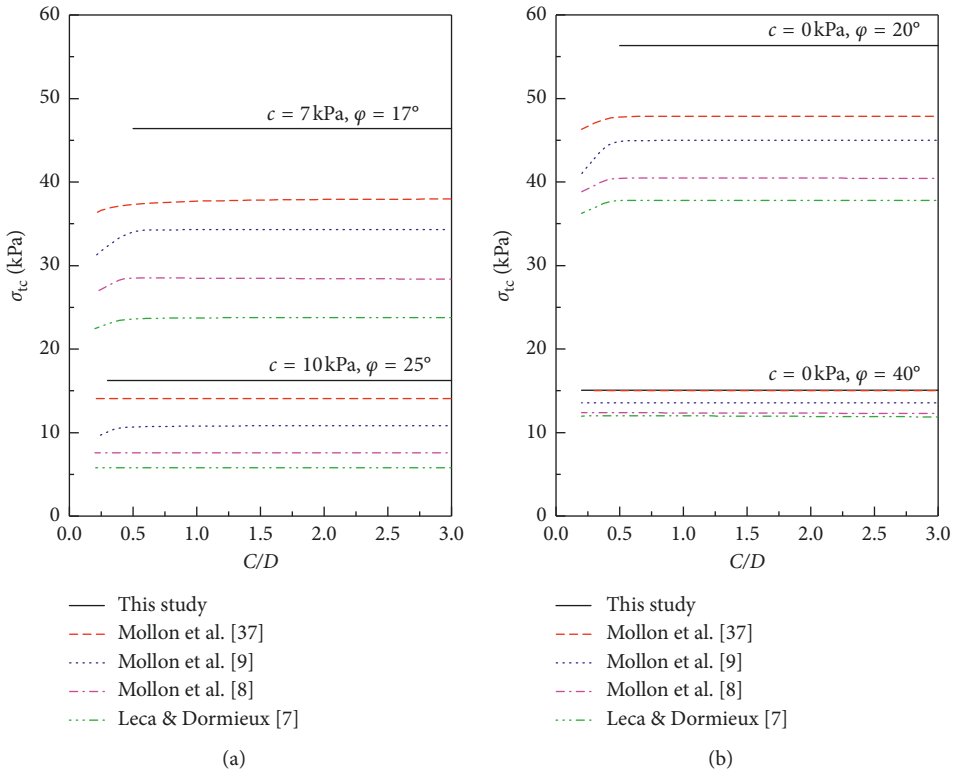

Figure 3: Comparisons of the critical results derived from different postulated mechanisms ($\gamma = 18$ kN/m^3 and $D = 10$ m).

Table 1: Comparisons of the obtained supported pressures (kPa) on the tunnel face for $D = 10$ m, $C = 10$ m, and $\gamma = 18$ kN/m^3.

		$c = 7$ kPa, $\varphi = 17^\circ$	$c = 10$ kPa, $\varphi = 25^\circ$
Numerical FD method	Mollon et al. [41]	37.3	12.2
	Zhang et al. [14]	32.5	11.7
Analytical LA method	Multiblock mechanism [8]	28.3	7.5
	Rotational mechanism [41]	37.8	13.9
	Truncated cone mechanism [41]	33.5	13.9
	Presented mechanism of this study	46.4	16.2

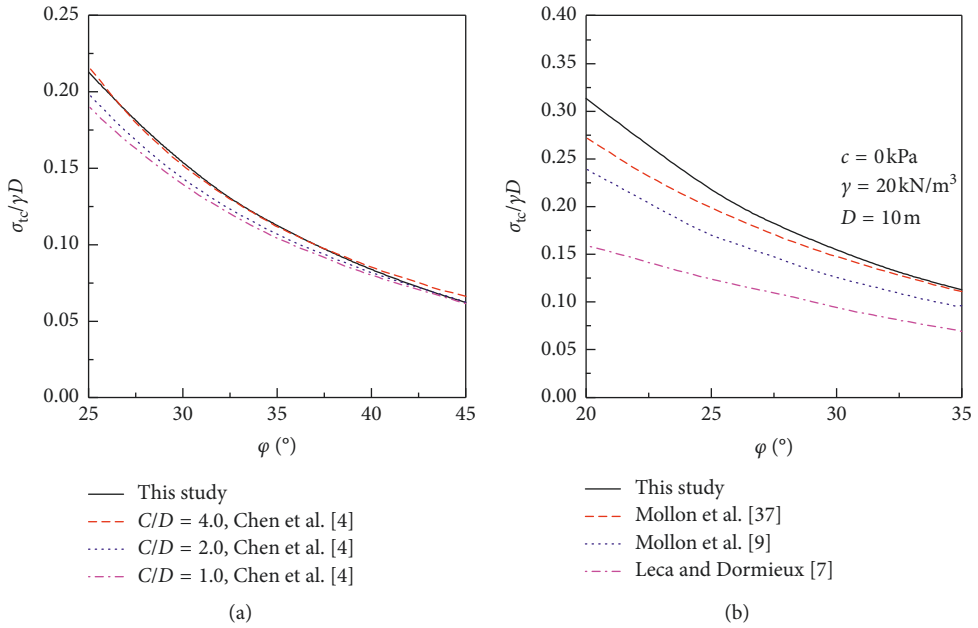

Figure 4: Comparisons of the critical results for tunnel face in cohesionless soils.

solutions for $C/D = 4$. Figure 4(b) illustrates the UB solutions derived from various mechanisms for purely frictional soils with different friction angles. The presented mechanism of this study yields the least upper bound on the support pressure. The differences of the UB solutions between this study and Mollon et al. [37] decrease with the increasing friction angle. Pan and Dias [32] employed the rotational failure mechanism of Mollon et al. [37] to obtain the support pressure of tunnel face subjected to pore water pressure. The approximate method based on the PWP coefficient was also used to calculate the upper bounds. These results are compared with the obtained UB solutions of this study, as shown in Figure 5. The presented mechanism can yield a greater value of the support pressure than the rotational mechanism of Mollon et al. [37]. As the height of the groundwater table increases, greater support pressure is required on the tunnel face. In addition, the UB solutions derived from the rotational mechanism by Wong and Subrin [29] are given here for comparisons, as shown in Table 2. The presented rotational mechanism of this study yields more critical results because of the improvement on the entirely inscribed circular face of the failure mechanism. Wong and Subrin [29] also carried out FD analysis to calculate the limit support pressure, but it is still less than the pressure presented in this study.

Using the optimization procedure can not only obtain the least upper bound of the support pressure but also the corresponding critical failure surface. Figures 6 and 7 illustrate the 3D geometry of the obtained critical failure mechanisms for the cohesive frictional soil and purely frictional soil, respectively. It can be seen that the overall failure surface is smooth and passing through the entire circular tunnel face. The failure surface for the purely frictional soil with $\varphi = 40^\circ$ is very similar to the observed failure surface from the experimental tests by Kirsch [25] and Berthoz et al. [30]. The 3D geometry of the proposed mechanism is close to the measured actual failure surface.

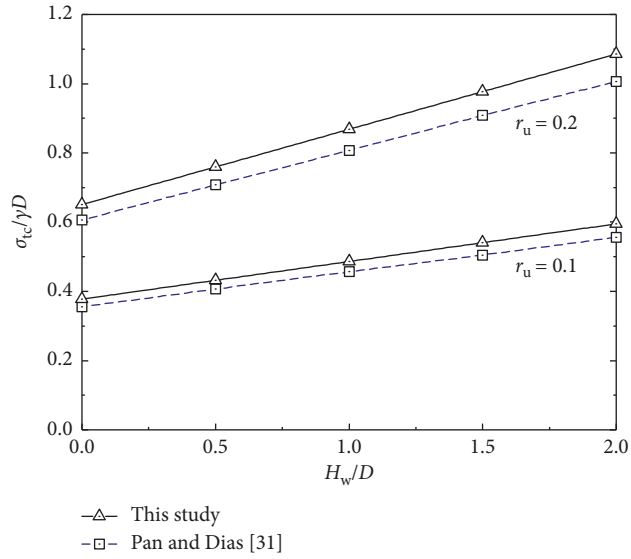

Figure 5: Comparison of the critical results for tunnel face subjected to pore water pressure ($c = 0$ kPa and $\varphi = 35^\circ$).

Table 2: Comparison of the calculated values of $\sigma_{tc}/\gamma D$ between this study and Wong and Subrin [29] for tunnels in purely frictional soils.

	Wong and Subrin [29]		This study
	UB solution	FD solution	UB solution
$\varphi = 10^\circ$	0.599	0.640	0.722
$\varphi = 20^\circ$	0.250	0.255	0.313
$\varphi = 30^\circ$	0.133	0.130	0.154

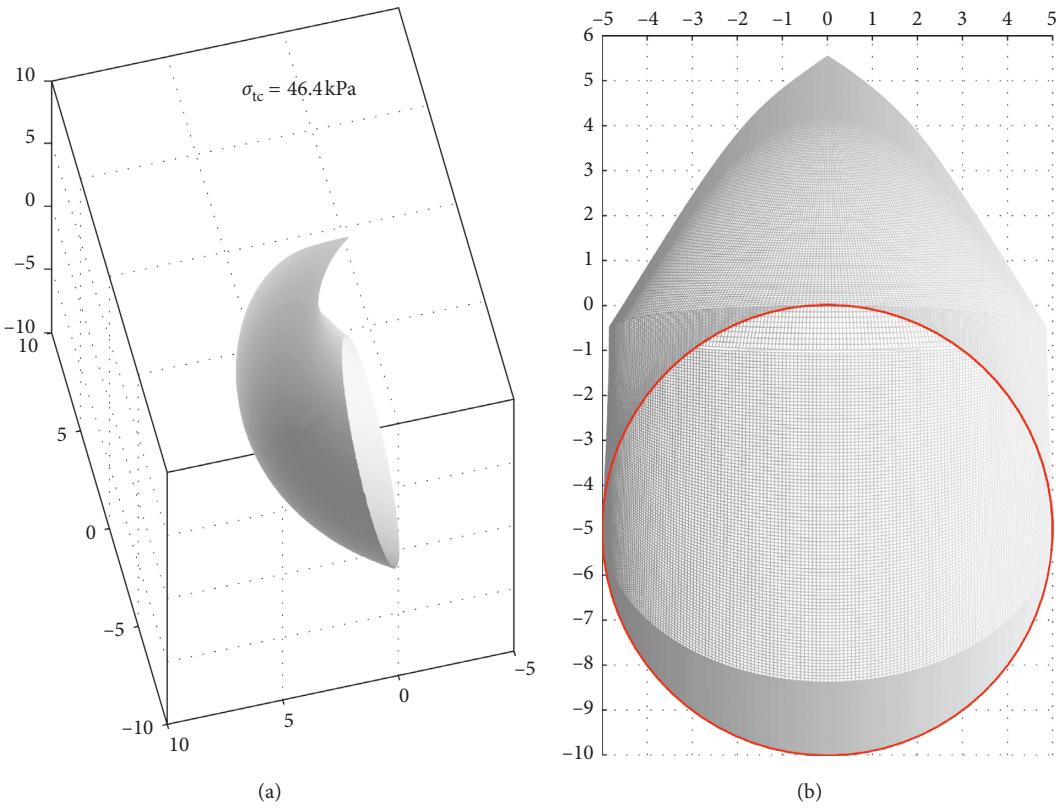

Figure 6: View of the critical failure surfaces of tunnel face in cohesive frictional soil with $c = 7$ kPa and $\varphi = 17^{\circ}$.

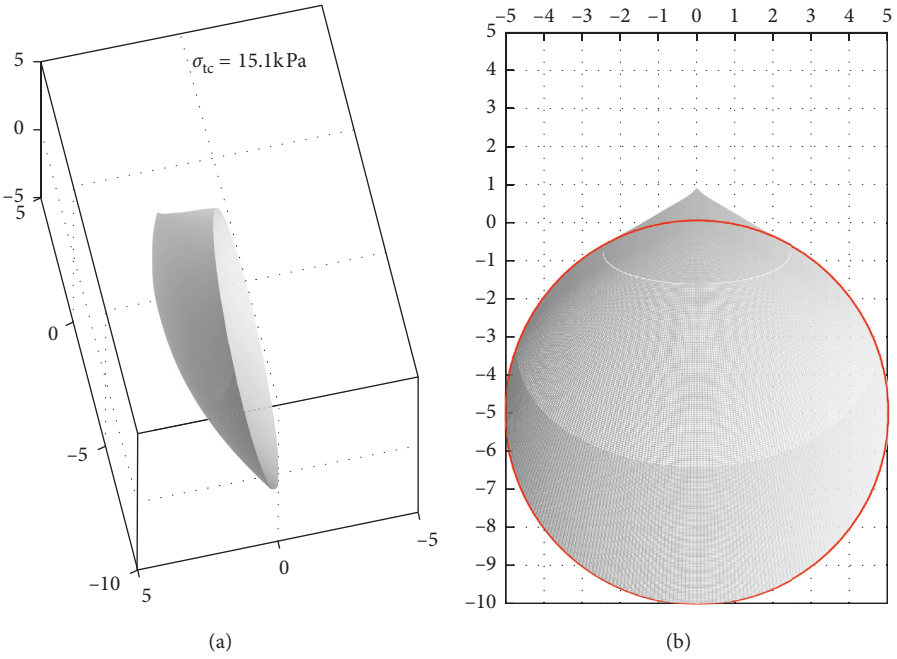

Figure 7: View of the critical failure surfaces of tunnel face in purely frictional soil with $c = 0$ kPa and $\varphi = 40^{\circ}$.

4.2. Stability Chart for Required Support Pressure. Through numerous calculations, the obtained UB solutions are presented in a stability chart, as shown in Figure 8. The chart provides a simple way to predict the required support pressure on circular faces of tunnels in frictional soil. It should be noted that the chart is limited to the collapse occurring below the ground surface. Figure 9 illustrates the heights of the critical failure surface from the tunnel crown.

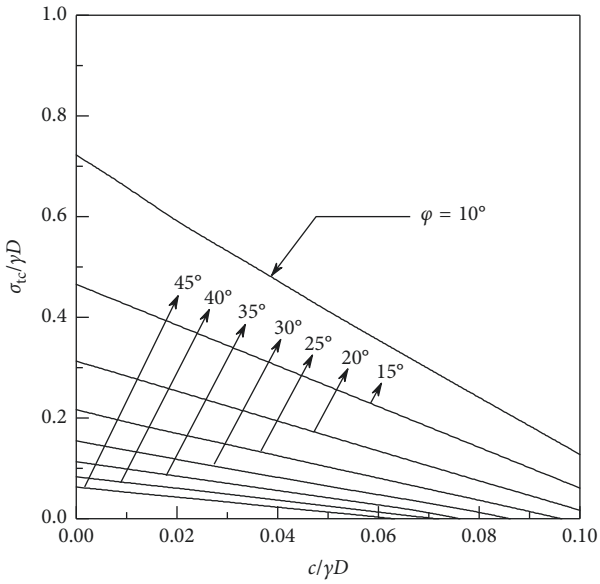

Figure 8: Stability charts of the critical pressure supported on the tunnel face.

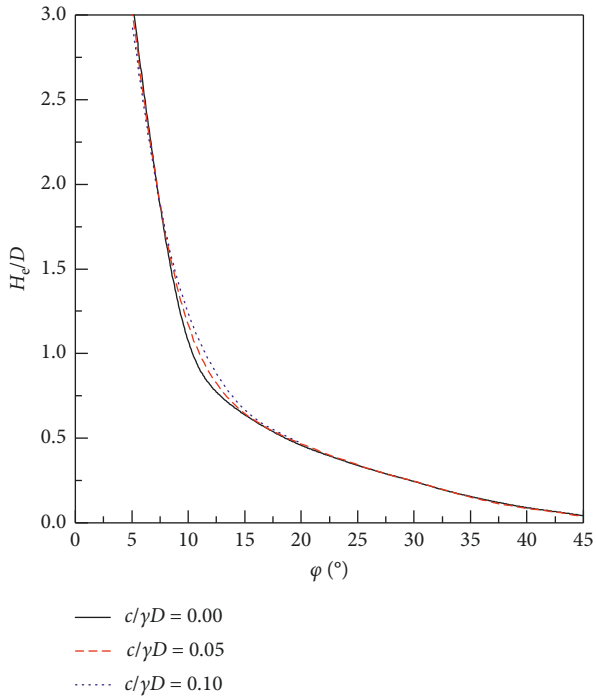

Figure 9: The critical heights of the tunnel face failures.

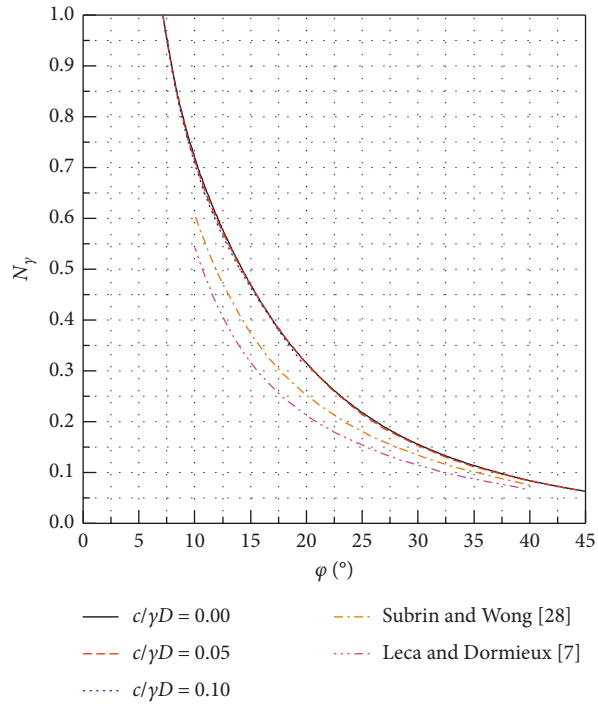

Figure 10: Dimensionless parameter N_γ for tunnel face stability.

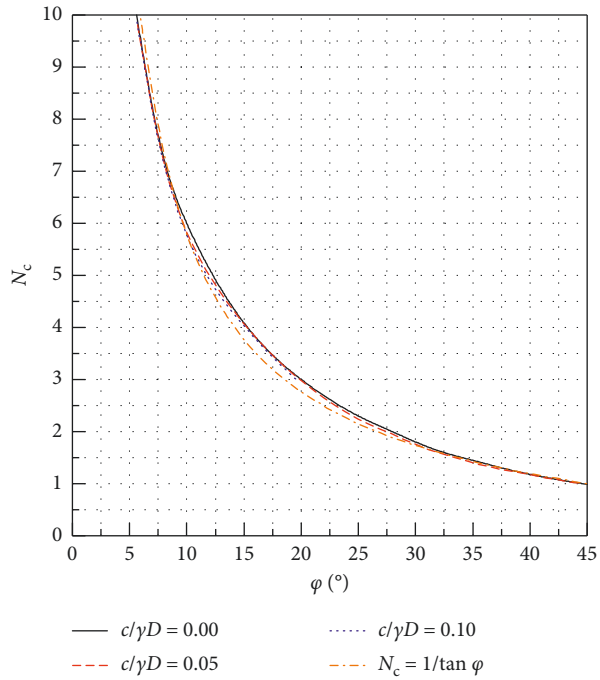

Figure 11: Dimensionless parameter N_c for tunnel face stability.

The height H_e reduces with the increasing friction angle. The cohesion of soil has insignificant influences on the height of the failure surface. When the friction angle φ is greater than 10°, the height of the critical failure surface cannot exceed the tunnel diameter. It implies that the presented chart can be used for $C \geq D$.

The coefficients N_γ and N_c in equation (20) are given for different friction angles, as shown in Figures 10 and 11, respectively. The friction angle has profound effects on the coefficients, but the influence of the soil cohesion is negligent. Compared with the values of N_γ given by Leca and Dormieux [7] and Subrin and Wong [28], this study can yield greater results. Subrin and Wong [28] obtained the coefficient $N_c = 1/\tan(\varphi)$ from their mechanism. As illustrated in Figure 11, the solutions of this study are close to their presented results. Reading the values of N_γ and N_c illustrated in Figures 10 and 11, we can obtain the required

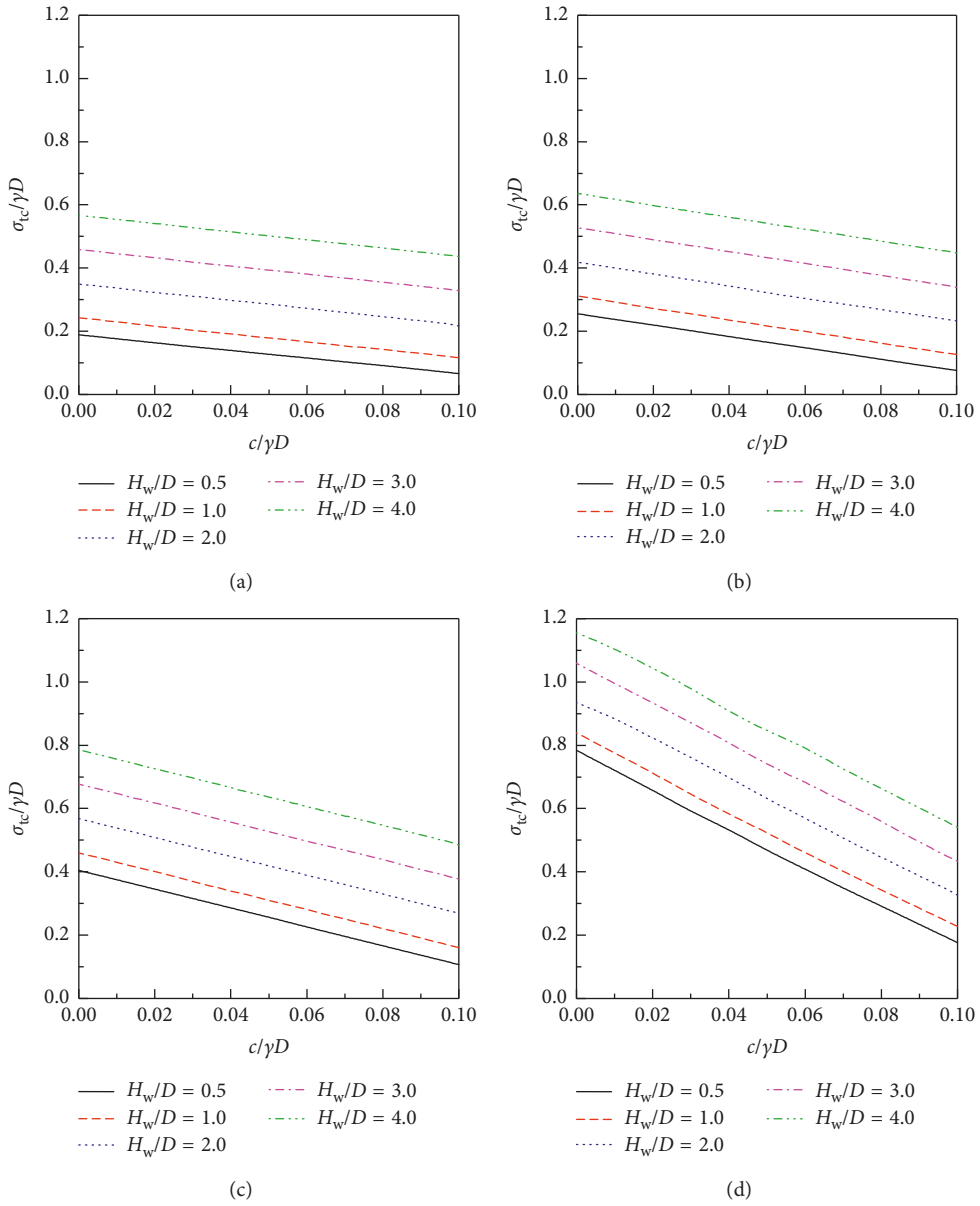

Figure 12: Stability charts of the critical pressure supported on the tunnel face under the pore water pressure $r_u = 0.1$. (a) $\varphi = 40^\circ$. (b) $\varphi = 30^\circ$. (c) $\varphi = 20^\circ$. (d) $\varphi = 10^\circ$.

support pressure through equation (20) for an arbitrary value of the friction angle.

Figures 12–14 show the stability charts for tunnel face subjected to pore water pressure with $r_u = 0.1$, 0.3, and 0.5, respectively. Several groundwater levels with $H_w/D = 0.5$, 1.0, 2.0, 3.0, and 4.0 are considered. As expected, the required support pressure increases with the increasing groundwater level. As the PWP coefficient increases to $r_u = 0.5$, the soil cohesion has a minor influence on the support pressure for greater friction angle. In this situation, the support pressure depends on the groundwater level. It should be noted that the PWP coefficient cannot be determined in practice and can only be used for approximate estimation. As presented by Pan and Dias [32], the numerical FE/FD analyses can be conducted to obtain the PWP distribution during the excavation and then incorporating it into the UB solutions could yield an accurate result.

5. Concluding Remarks

This study presents an improved rotational failure mechanism for circular faces of shield-driven tunnels in the frictional and/or cohesive soils. The mechanism has the shape of a curvilinear cone with an elliptical radial cross section and its lower and upper contours on the symmetry plane are defined by two log-spiral lines. Unlike the mechanism proposed by Subrin and Wong [28], it avoids the inscribed ellipse to the circular tunnel face and can involve the entire circular face of the tunnels. The generating 3D failure surface is kinematically admissible in LA, and using

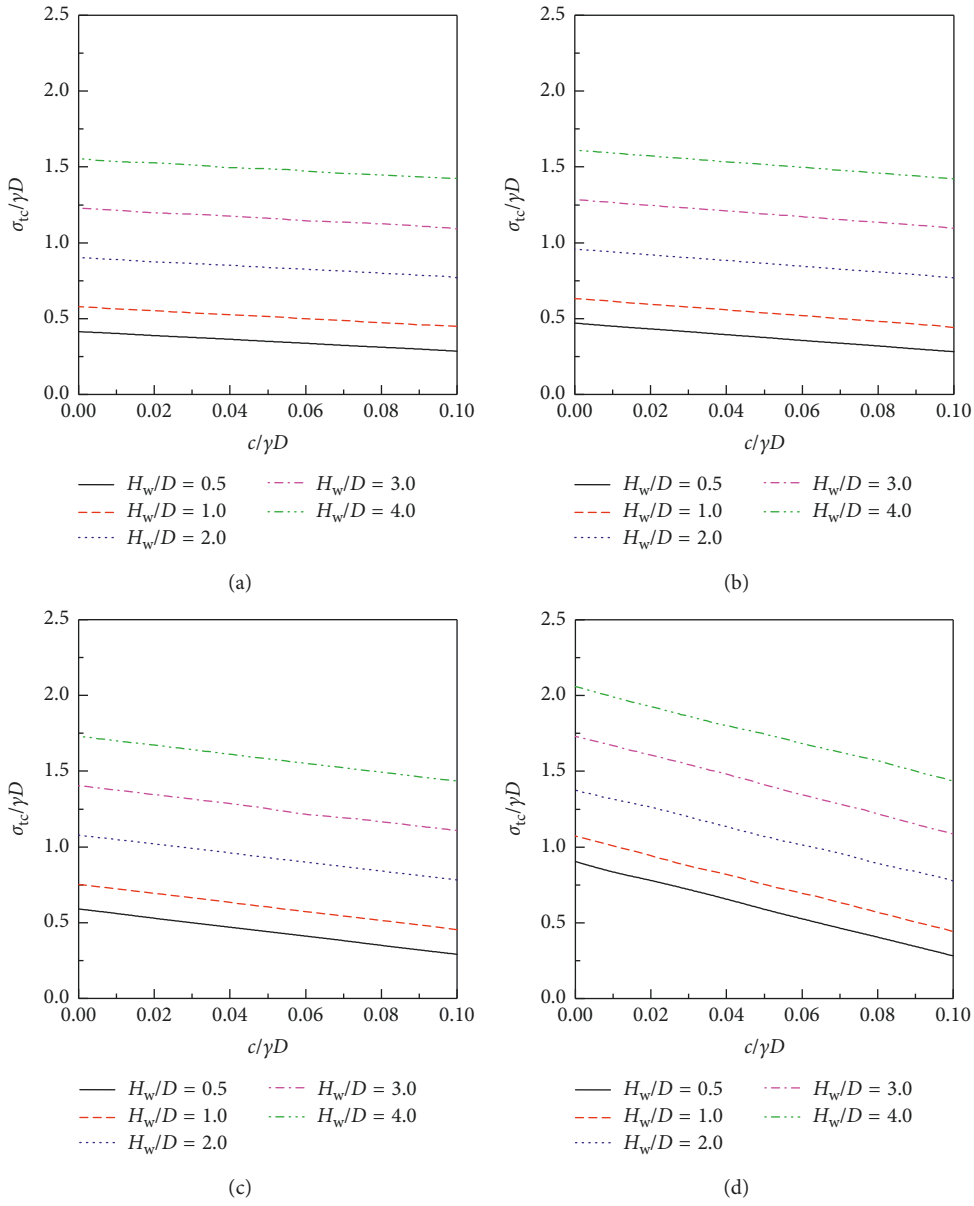

Figure 13: Stability charts of the critical pressure supported on the tunnel face under the pore water pressure $r_u = 0.3$. (a) $\varphi = 40^\circ$. (b) $\varphi = 30^\circ$. (c) $\varphi = 20^\circ$. (d) $\varphi = 10^\circ$.

the kinematic approach yields an upper bound to the support pressure on the tunnel face. Compared with the existing results derived from other mechanisms, the improved mechanism leads to the least UB solution in LA. It implies that the derived critical failure surface is closer to the actual one, as observed in some experimental tests.

Numerous calculations are carried out, and then the obtained UB solutions are presented in a stability chart. It provides a tool for convenient estimation of the required support pressure on circular faces of tunnels in frictional soils. The effects of the pore water pressure are also included in the stability analyses of tunnel faces. An approximate method based on the PWP coefficient is used to obtain the required support pressure on the face of shield-driven tunnels with a certain groundwater level. However, the value of the PWP coefficient cannot be determined in practice. When the PWP distribution during the excavations is derived from numerical FE/FD analyses, its involvement into the presented kinematical method can better estimate the limit support pressure.

The present mechanism can be further extended to tunnel face blowout, partial collapse on the tunnel face, and collapse reaching the ground surface in shallow tunnels. In fact, the modification on the elliptical cross section of the mechanism is not only suitable for the circular tunnel face but also used in other forms of the tunnel face, such as horseshoe and semiellipse. Although this study is limited to the frictional soil, the improvement of the rotational

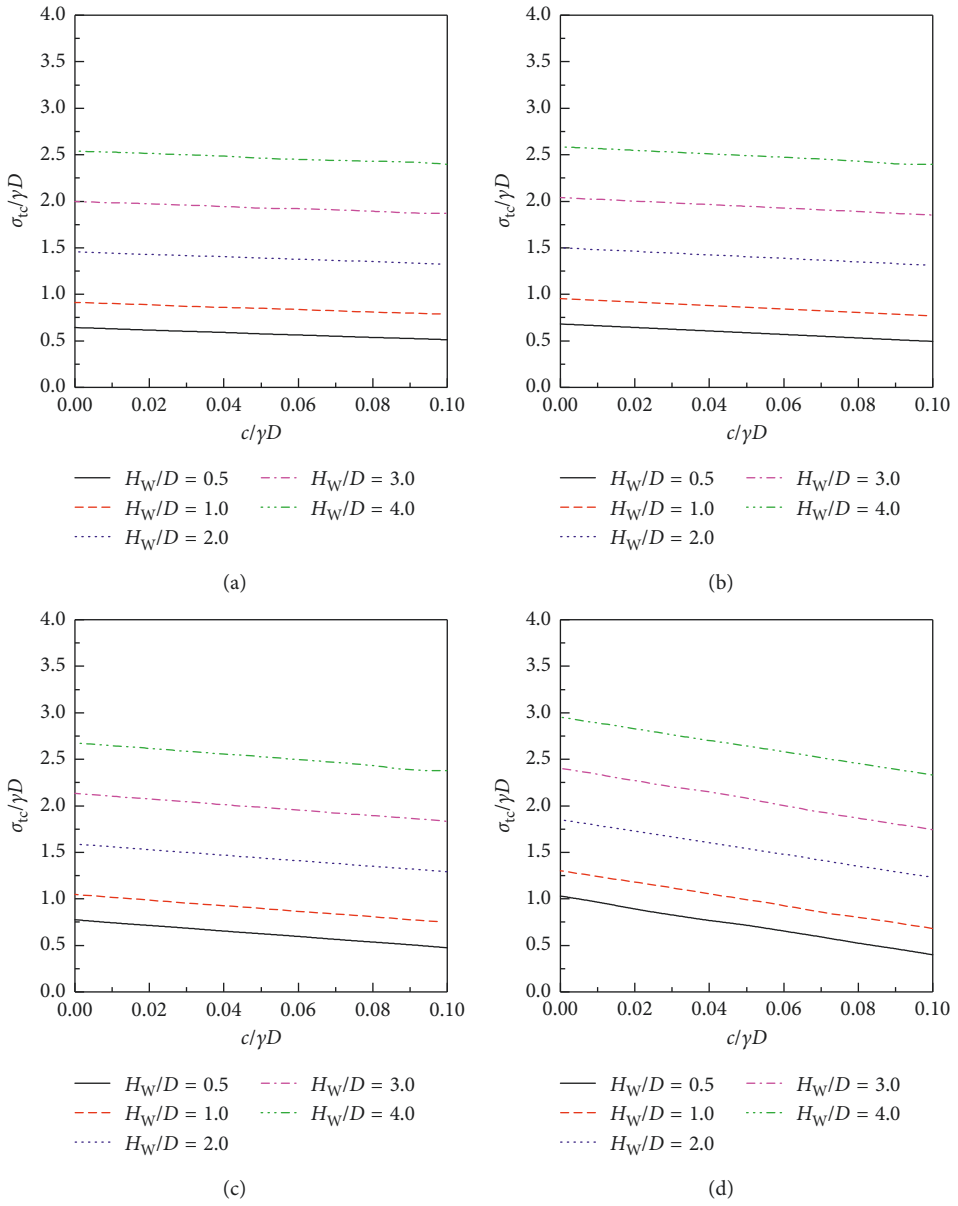

Figure 14: Stability charts of the critical pressure supported on the tunnel face under the pore water pressure $r_u = 0.5$. (a) $\varphi = 40^\circ$. (b) $\varphi = 30^\circ$. (c) $\varphi = 20^\circ$. (d) $\varphi = 10^\circ$.

mechanism could be useful in purely cohesive soil, as the continuous velocity field proposed by Mollon et al. [6]. Besides the tunnel face stability, the improved mechanism can be extended into other 3D geotechnical problems, such as slope stability and bearing capacity of footings.

Notations

a: Semimajor axis of an ellipse
b: Semiminor axis of an ellipse
C: Tunnel cover depth
c: Soil cohesion
D: Tunnel diameter
D_s: Rate of work dissipation
d_1, d_2: Parameters in equation (7)
e: Eccentricity of an ellipse
e_0: Eccentricity of the elliptic cross section at $\theta = \theta_{TU}$
H_w: Height of the groundwater table
H_e: Height of the failure surface from the tunnel crown
h_w: Depth of the failure surface below the groundwater table
N_γ, N_c, N_u: Dimensionless parameters
r, r': Radius of the lower and upper log-spiral lines
r_0: Log-spiral radius at $\theta = \theta_0$
r_m: Average radius of the two log spirals
r_u: Coefficient of pore water pressure
u: Pore water pressure
v: Radial velocity

W_γ: Work rate of soil weight
$W_{\sigma_{tc}}$: Work rate of supporting pressure on the tunnel face
W_u: Work rate of pore water pressure
γ: Unit weight of soil
η: Coefficient of the power function in equation (10)
θ: Angular coordinate in polar system
σ_{tc}: Supporting pressure on the tunnel face
φ: Internal friction angle of soils
ω: Angular velocity.

Data Availability

The data used to support the findings of this study are included within the article.

Conflicts of Interest

The authors declare that they have no conflicts of interest.

References

[1] N. Horn, "Horizontal earth pressure on the vertical surfaces of the tunnel tubes," in *Proceedings of National Conference of the Hungarian Civil Engineering Industry*, vol. 1, pp. 7–16, Budapest, Hungary, November 1961.

[2] G. Anagnostou and K. Kovári, "The face stability of slurry-shield-driven tunnels," *Tunnelling and Underground Space Technology*, vol. 9, no. 2, pp. 165–174, 1994.

[3] G. Anagnostou and K. Kovári, "Face stability conditions with earth-pressure-balanced shields," *Tunnelling and Underground Space Technology*, vol. 11, no. 2, pp. 165–173, 1996.

[4] R. P. Chen, L. J. Tang, X. S. Yin, Y. M. Chen, and X. C. Bian, "An improved 3D wedge-prism model for the face stability analysis of the shield tunnel in cohesionless soils," *Acta Geotechnica*, vol. 10, no. 5, pp. 683–692, 2015.

[5] A. Klar, A. S. Osman, and M. Bolton, "2D and 3D upper bound solutions for tunnel excavation using 'elastic' flow fields," *International Journal for Numerical and Analytical Methods in Geomechanics*, vol. 31, no. 12, pp. 1367–1374, 2007.

[6] G. Mollon, D. Dias, and A.-H. Soubra, "Continuous velocity fields for collapse and blowout of a pressurized tunnel face in purely cohesive soil," *International Journal for Numerical and Analytical Methods in Geomechanics*, vol. 37, no. 13, pp. 2061–2083, 2013a.

[7] E. Leca and L. Dormieux, "Upper and lower bound solutions for the face stability of shallow circular tunnels in frictional material," *Géotechnique*, vol. 40, no. 4, pp. 581–606, 1990.

[8] G. Mollon, D. Dias, and A.-H. Soubra, "Probabilistic analysis and design of circular tunnels against face stability," *International Journal of Geomechanics*, vol. 9, no. 6, pp. 237–249, 2009.

[9] G. Mollon, D. Dias, and A.-H. Soubra, "Face stability analysis of circular tunnels driven by a pressurized shield," *Journal of Geotechnical and Geoenvironmental Engineering*, vol. 136, no. 1, pp. 215–229, 2010.

[10] K. Han, C. Zhang, W. Li, and C. Guo, "Face stability analysis of shield tunnels in homogeneous soil overlaid by multilayered cohesive-frictional soils," *Mathematical Problems in Engineering*, vol. 2016, Article ID 1378274, 9 pages, 2016.

[11] N. Khezri, H. Mohamad, M. HajiHassani, and B. Fatahi, "The stability of shallow circular tunnels in soil considering variations in cohesion with depth," *Tunnelling and Underground Space Technology*, vol. 49, no. 7, pp. 230–240, 2015.

[12] I.-M. Lee, S.-W. Nam, and J.-H. Ahn, "Effect of seepage forces on tunnel face stability," *Canadian Geotechnical Journal*, vol. 40, no. 2, pp. 342–350, 2003.

[13] X.-W. Tang, W. Liu, B. Albers, and S. Savidis, "Upper bound analysis of tunnel face stability in layered soils," *Acta Geotechnica*, vol. 9, no. 4, pp. 661–671, 2014.

[14] C. Zhang, K. Han, and D. Zhang, "Face stability analysis of shallow circular tunnels in cohesive-frictional soils," *Tunnelling and Underground Space Technology*, vol. 50, pp. 345–357, 2015.

[15] L. Zhao, D. Li, L. Li, F. Yang, X. Cheng, and W. Luo, "Three-dimensional stability analysis of a longitudinally inclined shallow tunnel face," *Computers and Geotechnics*, vol. 87, pp. 32–48, 2017.

[16] J.-F. Zou, A. Wei, and T. Yang, "Elasto-plastic solution for shallow tunnel in semi-infinite space," *Applied Mathematical Modelling*, vol. 64, no. 12, pp. 669–687, 2018.

[17] J.-F. Zou, Z.-H. Qian, X.-H. Xiang, and G. H. Chen, "Face stability of a tunnel excavated in saturated nonhomogeneous soils," *Tunnelling and Underground Space Technology*, vol. 83, no. 2, pp. 1–17, 2019.

[18] J. F. Zou, L. Liu, and M. Y. Xia, "A new simple approach for the quasi-plane strain problem of circular tunnel in strain-softening rock mass incorporating the effect of out-of-plane stress," *Acta Geotechnica*, 2019.

[19] J.-f. Zou, Z.-h. Qian, X.-h. Xiang, and G. H. Chen, "Face stability of a tunnel excavated in saturated nonhomogeneous soils," *Tunnelling and Underground Space Technology*, vol. 83, no. 1, pp. 1–17, 2019.

[20] J. F. Zou, F. Wang, and A. Wei, "A semi-analytical solution for shallow tunnels with radius-iterative-approach in semiinfinite space," *Applied Mathematical Modelling*, 2019.

[21] J. F. Zou and P. H. Zhang, "Analytical model of fully grouted bolts in pull-out tests and in situ rock masses," *International Journal of Rock Mechanics and Mining Sciences*, vol. 113, no. 1, pp. 278–294, 2019.

[22] D. Takano, J. Otani, H. Nagatani, and T. Mukunoki, "Application of x-ray CT on boundary value problems in geotechnical engineering: research on tunnel face failure," in *Proceedings of GeoCongress 2006: Geotechnical Engineering in the Information Technology Age*, vol. 1, pp. 1–6, Atlanta, GA, USA, February 2006.

[23] M. Ahmed and M. Iskander, "Evaluation of tunnel face stability by transparent soil models," *Tunnelling and Underground Space Technology*, vol. 27, no. 1, pp. 101–110, 2012.

[24] G. Idinger, P. Aklik, W. Wu, and R. I. Borja, "Centrifuge model test on the face stability of shallow tunnel," *Acta Geotechnica*, vol. 6, no. 2, pp. 105–117, 2011.

[25] A. Kirsch, "Experimental investigation of the face stability of shallow tunnels in sand," *Acta Geotechnica*, vol. 5, no. 1, pp. 43–62, 2010.

[26] W. Liu, Y. Zhao, P. Shi, J. Li, and P. Gan, "Face stability analysis of shield-driven tunnels shallowly buried in dry sand using 1-g large-scale model tests," *Acta Geotechnica*, vol. 13, no. 3, pp. 693–705, 2017.

[27] X. Lü, Y. Zhou, M. Huang, and S. Zeng, "Experimental study of the face stability of shield tunnel in sands under seepage condition," *Tunnelling and Underground Space Technology*, vol. 74, pp. 195–205, 2018.

[28] D. Subrin and H. Wong, "Stabilité du front d'un tunnel en milieu frottant :t un nouveau mécanisme de rupture 3D," *Comptes Rendus Mécanique*, vol. 330, no. 7, pp. 513–519, 2002.

[29] H. Wong and D. Subrin, "Stabilité frontale d'un tunnel Mécanisme 3D en forme de corne et influence de la profondeur," *Revue Européenne de Génie Civil*, vol. 10, no. 4, pp. 429–456, 2006.

[30] N. Berthoz, D. Branque, D. Subrin, H. Wong, and E. Humbert, "Face failure in homogeneous and stratified soft ground: theoretical and experimental approaches on 1g EPBS reduced scale model," *Tunnelling and Underground Space Technology*, vol. 30, no. 4, pp. 25–37, 2012.

[31] Q. Pan and D. Dias, "Face stability analysis for a shield-driven tunnel in anisotropic and nonhomogeneous soils by the kinematical approach," *International Journal of Geomechanics*, vol. 16, no. 3, article 04015076, 2016a.

[32] Q. Pan and D. Dias, "The effect of pore water pressure on tunnel face stability," *International Journal for Numerical and Analytical Methods in Geomechanics*, vol. 40, no. 15, pp. 2123–2136, 2016b.

[33] Q. Pan and D. Dias, "Upper-bound analysis on the face stability of a non-circular tunnel," *Tunnelling and Underground Space Technology*, vol. 62, pp. 96–102, 2017a.

[34] Q. Pan and D. Dias, "Probabilistic evaluation of tunnel face stability in spatially random soils using sparse polynomial chaos expansion with global sensitivity analysis," *Acta Geotechnica*, vol. 12, no. 6, pp. 1415–1429, 2017b.

[35] Q. Pan and D. Dias, "Three dimensional face stability of a tunnel in weak rock masses subjected to seepage forces," *Tunnelling and Underground Space Technology*, vol. 71, pp. 555–566, 2018.

[36] A. Drescher, "Kinematics of axisymmetric vertical slopes at collapse," *International Journal for Numerical and Analytical Methods in Geomechanics*, vol. 10, no. 4, pp. 431–441, 1986.

[37] G. Mollon, D. Dias, and A.-H. Soubra, "Rotational failure mechanisms for the face stability analysis of tunnels driven by a pressurized shield," *International Journal for Numerical and Analytical Methods in Geomechanics*, vol. 35, no. 12, pp. 1363–1388, 2011.

[38] R. L. Michalowski, "Slope stability analysis: a kinematical approach," *Géotechnique*, vol. 45, no. 2, pp. 283–293, 1995.

[39] R. L. Michalowski and S. S. Nadukuru, "Three-dimensional limit analysis of slopes with pore pressure," *Journal of Geotechnical and Geoenvironmental Engineering*, vol. 139, no. 9, pp. 1604–1610, 2013.

[40] A. W. Bishop and N. Morgenstern, "Stability coefficients for earth slopes," *Géotechnique*, vol. 10, no. 4, pp. 129–153, 1960.

[41] G. Mollon, D. Dias, and A.-H. Soubra, "Range of the safe retaining pressures of a pressurized tunnel face by a probabilistic approach," *Journal of Geotechnical and Geoenvironmental Engineering*, vol. 139, no. 11, pp. 1954–1967, 2013b.